A Self-Adaptive Fractional Order PID Controller for the Particle Velocity Regulation in a Pneumatic Conveying System

Faisal Abbas, Omer Saleem, Lijuan Wang, Yong Yan

***Abstract*—This paper presents the methodical development of a state-error-driven self-adaptive Fractional Order PID (AFOPID) control algorithm to efficiently regulate the velocity of pneumatically conveyed particles at the desired set point as well as to prevent the blockage of particles in a pipe due to an imbalanced combination of their velocity and corresponding mass flow rate. The proposed fractional control law is constituted by adaptively modulating fractional orders of the integral and differential operators in the control based on the state-error variations in the velocity of solid particles. The particle's velocity is measured and updated via electrostatic sensors in conjunction with cross-correlation signal processing algorithms. All the other fixed hyper-parameters associated with the PID control scheme are meta-heuristically optimized by using a genetic algorithm. The proposed AFOPID is benchmarked against conventional integer-order PID and the Fractional Order PID (FOPID) controllers. Experiments are performed on a laboratory-scale test rig to comparatively analyze the aforesaid control schemes; where each controller is examined for three velocity set points and three disturbance levels. The experimental results validate the superior time-optimality and robustness of the proposed AFOPID controller against bounded disturbances and abrupt velocity set-point variations by manifesting relatively faster settling time, low overshoots (and undershoots), and smaller steady-state fluctuations.**

***Index Terms*—Adaptive Fractional Order PID, Genetic Algorithm, PID, Velocity control**

I. INTRODUCTION

Two-phase gas-solid flow systems are widely seen in many industrial processes such as food processing, handling of fertilizers in agricultural cycles, cement production, shipping, and power generation [Yan et al. (2021)]. One of the most commonly seen examples of such a system is the pneumatically conveyed pulverized coal particles in the fuel lines of coal-fired power plants [Qian et al. (2017)]. Applications of pneumatic conveying systems for handling bulk solids are undergoing rapid growth as they can significantly enhance the efficiency of material transportation, prevent environmental pollution, and boost manufacturing safety and reliability. However, the complex flow patterns in pneumatic conveying pipelines create intricate modeling and measurement challenges [Yan (1996)]. An uncontrolled flow rate is wasteful, as it can either lead to energy wastage or eventually result in an unscheduled shutdown of the plant due to a deficiency of fuel.

To avoid these circumstances, the transportation of material through pipes should be optimized, which generally requires the flow rate to be controlled within a certain range. Measuring the velocity of solid particles in the aforementioned industrial processes is very important, as the product of velocity and concentration results in the mass flow rate of solid particles, which is required to control the efficiency of the process. Furthermore, velocity measurement is an important factor in evaluating pipeline erosion, as erosion is directly proportional to velocity and concentration [Xu et al. (2018)]. Also, in some industrial processes, it is observed that an uncontrolled and imbalanced amount of velocity and mass flow rate of these solid particles can sometimes block the pipe, which eventually results in a catastrophic situation. As the velocity of solid particles plays an important role in determining the above-mentioned factors, it is therefore highly desirable to develop such agile control schemes that can flexibly regulate the velocity of ongoing solid particles whenever the system encounters a blockage or any kind of disturbance problem inside a pneumatic pipe.

A. Literature Review

Pneumatic conveying systems are widely used in industries for transporting bulk materials through pipelines using air or another gas [Abe et al. (2023), Klinzing et al. (2015)]. Control of particle velocity in these systems is critical for ensuring efficiency, minimizing wear and tear, reducing energy consumption, and preventing blockages or damage to the materials being conveyed [Weber and Molerus (1990)]. Pneumatic conveying can be broadly classified into dilute-phase and dense-phase systems [Wypych (1995)]. Dilute-phase conveying involves transporting particles suspended in the conveying gas at high velocities, whereas dense-phase conveying operates at lower velocities with particles moving in a more plug-like manner [Mills (2004)].

Developing and incorporating agile closed-loop particle-velocity control techniques with pneumatic conveying systems is also crucial for the said industrial processes. However, this development depends on the availability of accurate velocity measurements so that they can be fed back to the closed-loop controller. Hence, it is of utmost importance to discuss the state-of-the-art velocity measurement and acquisition methods that are available in the open literature and discuss their suitability for the proposed control system development. A variety of sensor paradigms have been proposed for monitoring particle velocity and concentration in a bulk strong pneumatic conveyor scheme, including radiometric [Barratt et al. (2000)], capacitive [Zhang et al. (2012)], ultrasonic [Zulkiflli et al. (2019)], optical [Qian et al. (2015)], microwave [Penirschke et al. (2008)], and heat transfer methods. All these sensors are non-intrusive and can monitor the velocity as well as the concentration of particles. However, their usage poses challenges in some cases. Radiometric devices pose a serious threat to the user's health and safety. The capacitive sensor measurements tend to get corrupted by the dielectric properties of the material(s) being monitored. The optical detectors require a transparent window in the pipe that is prone to pulverized material contamination and abrasion. The ultrasonic sensors are susceptible to error-induced false signals. Finally, the microwave sensors work with moderate accuracy at the cost of being

very expensive. Electrostatic charge-based sensing devices are preferred due to their simple design, cost-effectiveness, durability, and robustness [Yan et al. (1995), Coombes & Yan (2016)]. Owing to their aforementioned attributes, non-invasive electrostatic sensors are adopted in this work to accurately analyze the flow conditions of solid particles in the pipe without disturbing flow dynamics.

A lot of attempts have been made in the literature to develop robust particle velocity regulation schemes for pneumatic conveying systems. The PLC-based automatic control system for pneumatic conveying systems, proposed in [Genxi et al. (2008)], lacks the design flexibility to address the system's state error deviations. Proportional-Integral-Derivative (PID) controllers are widely favored due to their simple structure and reliable yield to control industrial processes [Bequette (2003)]. A PI control system assisted by tomographic imaging was developed to control the particle velocity in the conveying system [Deloughry et al. (2001)]. However, it lacked the robustness to address rapid variations in setpoint velocity and random disturbances. The sliding-mode controllers tend to deliver robust control effort at the cost of highly discontinuous control activity and increased chattering content in the state response [Ren, Wang, Fan & Kaynak (2019)]. Despite their design flexibility, fuzzy controllers require an elaborate set of qualitative rules that are empirically synthesized based on the expert's knowledge and, hence, are bound to contain inaccuracies [Barbosa & Seleghim (2011), Neuffer et al. (1999)]. The statistical control scheme presented in [Ramonowski et al. (2006)] uses statistical Bayesian modeling combined with a Markov chain Monte Carlo (MCMC) sampling algorithm to analyze the data and generate appropriate control commands. The fuzzy-PID control scheme proposed in [Sun et al. (2022)] yields fast, stable, and high-precision flow control in the pneumatic conveying system. To improve the controller's adaptability to efficiently reject the exogenous disturbances, a neural network-based controller is employed that tracks a well-postulated gain-scheduled PID reference controller to yield robust control effort [Barbosa & Seleghim (2003)]. The simulation results show that the proposed scheme yields a 50% improvement in power

efficiency as compared to the conventional control schemes. The multivariable controllers have also been rigorously analyzed for pneumatic conveying of particulate material [Birk (1999)]. Despite their optimality, model predictive controllers (MPCs) rely upon a multitude of parameters that require accurate tuning [Jones and Jabob (2007)]. The nonlinear MPCs have demonstrated enhanced reference tracking accuracy and a reasonably enhanced closed-loop response with minimal control effort [Satpati et al. (2014)]. However, they require complex computational algorithms for their realization. An optimal control design for the pneumatic conveying system is presented in [Wilms and Dhodapkar (2014)]. However, its performance is prone to degradation under parametric uncertainties.

To address the shortcomings of state-of-the-art control schemes, fractional calculus is integrated with the integer-order PID controller to formulate the Fractional Order PID (FOPID) controller [Shekher et al. (2012), Erenturk (2013)]. This scheme is widely preferred for controlling nonlinear and chaotic systems [Ren, Fan & Kaynak (2019), Zhang & Pi (2012), Giernacki (2016)]. In addition to the PID gains, the FOPID controller introduces two new parameters (δ, μ) that serve as its integral and derivative operator's fractional orders [Mishra & Chandra (2014)]. These fractional operators increase the controller's degree of freedom and design flexibility [Dumlu & Erenturk (2014)]. The performance of the ubiquitous FOPID controllers can be further enhanced by adaptively modifying the parameters (δ, μ) via an online parameter adaptation mechanism [Saleem & Abbas (2017), Saleem et al. (2020)]. Different variants of adaptive FOPID controllers have been observed to yield promising results by improving the robustness of closed-loop energy-conversion and electro-mechanical systems against exogenous disturbances [Saleem & Abbas (2017), Saleem et al. (2020), Saleem & ul Hasan (2019)].

B. Main Contributions

The main contribution of this paper is the formulation of a well-postulated adaptive FOPID (AFOPID) controller to regulate the velocity of solid particles in a pneumatic conveying system. The proposed control procedure is realized by augmenting the conventional FOPID controller with an online adaptation mechanism that serves as a superior regulator to dynamically adjust the fractional orders in real-time. The key contributions of this article are thus listed below:

- Constitution of the baseline FO-PID controller for a pneumatic conveying system.
- Realization of the proposed adaptive FO-PID controller by retrofitting it with an online adaptation law.
- Formulation of the adaptation law by employing a pre-configured nonlinear hyperbolic secant function that depends on the real-time error variations in the particle velocity. These functions are formulated via well-established meta-rules that self-tune the fractional power to speed up the transient response and alter the damping control force as the error conditions change, respectively.
- Experimentally validating the efficacy of the designed controller variants by conducting real-time experiments on a standard pneumatic conveying hardware setup.

The proposed AFOPID controller is benchmarked against the conventional PID and FOPID to justify its efficacy. The proportional, integral, and derivative gains of the three aforesaid controller variants are meta-heuristically tuned offline via the Genetic Algorithm (GA) and are kept constant during every experimental trial [26]. The performance of the proposed control scheme is validated by conducting customized real-time hardware-in-the-loop experiments on a pneumatic conveying test rig. The experimental results and the corresponding comparative analysis, presented later in the article, also validate that the proposed methodology can effectively regulate the velocity of solid particles at the specified set point with cross-correlation as a velocity measurement method using two ring-shaped flush-mounted electrostatic sensors. The robustness of the

implemented system is also validated by introducing three levels of disturbances in the system's steady-state response.

C. Features of the Proposed Scheme

There are several advantages to using the proposed control procedure. Fractional controllers are suitable to realize and address the intrinsic nonlinear dynamics and chaotic behavior of physical systems. The introduction of self-tuning fractional orders increases the controller's degree-of freedom and flexibility of controller design, which enhances the system's robustness against random exogenous disturbances. The self-tuning fractional orders achieve the aforesaid control objective by smoothly alternating the fractional controller to act predominantly like a PD controller under large error (transient) conditions to damp the overshoots and ensure a rapid transit, and like a PI controller as the response converges to the setpoint to minimize the steady-state fluctuations. This is indeed an innovative feat. Additionally, the nonlinear scaling functions formulated to adaptively self-tune the fractional orders can be algebraically solved in a single step after every sampling interval, which does not put any recursive computational burden on the processor. Hence, the proposed scheme can be realized using modern digital computers. The bounded variation of the fractional orders dictated by the nonlinear functions also serves to preserve the system's closed-loop stability.

As compared to the traditional PID controllers, the FOPID controllers introduce two additional parameters (fractional orders of the integral and derivative terms), providing more flexibility to handle external disturbances. However, the tuning of these parameters is generally quite labor-intensive. The proposed controller addresses this issue by adaptively modulating the fractional orders. Apart from yielding better performance in adapting to changing system dynamics, this arrangement obviates the necessity to offline optimize the said parameters. However, the fractional calculus in conjunction with the adaptive system results

in slightly higher computational requirements. But modern digital computers have sufficient processing power to handle the computational burden. The SMCs are simpler to implement, but the smooth dynamic adjustment of the fractional orders in the proposed controller results in generating smoother control actions, thus, deliberately avoiding the chattering problem.

Unlike the LQRs, the model-free nature of the proposed controller enables it to effectively handle the intrinsic nonlinearities and model uncertainties. Its implementation is quite easier for systems whose precise mathematical model is either not available or is difficult to derive. However, its control effort may be suboptimal in terms of a quadratic cost function. The MPC solves optimization problems online, which inevitably makes it computationally expensive. The proposed scheme requires relatively less computational resources compared to MPC. The translation of expert knowledge into fuzzy rules simplifies the fuzzy control design. However, the definition of these heuristic rules or their tuning may not always be precise, which degrades the controller's performance. On the contrary, the proposed controller provides a clear analytical framework for design and tuning. Unlike the neural controllers, the proposed scheme can adapt to reject disturbances in the system in real-time without extensive training, which makes it computationally simpler. The proposed controller indeed possesses some shortcomings as compared to the existing control schemes. However, its benefits tend to outweigh its limitations.

The idea of using an adaptive FOPID controller with self-tuning fractional orders to robustly regulate the particle velocity in a pneumatic conveying system under disturbances has never been attempted in the scientific literature. Hence, the proposed scheme is novel and innovative.

The remaining paper is organized as follows: The measurement system is described in Section II. The proposed control scheme is formulated in Section III. The parameter optimization methodology is discussed in Section IV. The experimental analysis is presented in Section V. The article is concluded at the end.

II. PARTICLE VELOCITY ESTIMATION SYSTEM

As discussed earlier, pneumatic conveying systems are significant in various industries due to their efficiency, flexibility, and reliability to handle a wide range of materials. They enhance operational efficiency, ensure product quality, and contribute to safer and more sustainable industrial practices. However, developing a robust and agile control system that regulates the particle velocity in the system poses a challenging problem for the scientists. However, it is imperative to derive a mathematical model of the particle motion in the conveying system to analyze the dynamics of the system and then develop a suitable control scheme around it. This section presents a nominal model of particle motion as well as a comprehensive description of the particle velocity determination system.

A. Mathematical Model of Particle Motion

To model the system dynamics of a particle flowing in a fluid, consider a constant horizontal input force T applied to a spherical inertial particle as it travels across a pneumatic conveying channel. The one-dimensional equation of motion of a particle having mass m subject to a drag force F_d is expressed as given below [18].

$$m\dot{v} = F_d + T \tag{1}$$

where, v represente the particle's velocity in the inertial frame, $\dot{v}$ is the particle's acceleration, is T is the constant thrust force input. Ideally, the particle is subjected to a linear Stokes drag force, as shown in (2).

$$F_d = -3\pi d\rho(v - w) \tag{2}$$

where, d is the diameter of the spherical particle, ρ is the dynamic viscosity of the fluid (air in this case) at room temperature, and w is the velocity of the fluid flow in the inertial frame. By substituting Equation (2) in (1), the first-order differential equation representing the particle motion dynamics is formulated as given below.

$$\dot{v} = -\left(\frac{3\pi d\rho}{m}\right)v + \left(\frac{3\pi d\rho}{m}\right)w + \left(\frac{1}{m}\right)T \tag{3}$$

Assuming that the velocity of fluid flow w is negligible, the aforementioned expression can be simplified as shown in (4).

$$\dot{v} = -\left(\frac{3\pi d\rho}{m}\right)v + \left(\frac{1}{m}\right)T \tag{4}$$

The expression resembles the state equation of a linear dynamic system $\dot{x} = ax + bu$; where, $x = v$ is the state variable, $a = -\frac{3\pi d\rho}{m}$ is the system variable, $b = \frac{1}{m}$, and $u = T$ is the system's input. The transfer function of the system for $v(0) = 0$ at is expressed in (5).

$$G(s) = \frac{V(s)}{T(s)} = \frac{1}{ms + 3\pi d\rho} \tag{5}$$

where, s is the Laplace operator. In this work, the pneumatic conveyance of fine wheat flour particles is used for experimentation. The model parameters are shown in Table I [29].

TABLE I

Identification of System Parameters

Symbol	Description	Value	Unit
m	Mass of the particle	2.48×10-9	kg
d	Diameter of the particle	200	μm
ρ	Dynamic viscosity of the fluid (air)	1.85×10-5	kg/m.s

B. Cross-Correlation Scheme for Particle Velocity Estimation

The cross-correlation technique is used to evaluate the likelihood between two signals, $q_1(t)$ and $q_2(t)$, as a function of the time delay τ_p between them. These signals are acquired via two transducers that are deployed

upstream and downstream in the pipe at a fixed distance from each other. The cross-correlation R_{12} of the acquired signals is computed as shown in (6) [Zhang et al. (2016)].

$$R_{12}(p) = \frac{\sum_{k=1}^{N} q_1(i) q_2(i+p)}{\left(\sqrt{\sum_{k=1}^{N} q_1^2(i)}\right)\left(\sqrt{\sum_{k=1}^{N} q_2^2(i)}\right)} \tag{6}$$

where, N is the number of sampling points, P is the maximum number of delayed points p ($P = 0, 1, 2, \dots, p$), and $q_1(i)$ and $q_2(i)$ represent the discretized signals, $q_1(t)$ and $q_2(t)$, respectively. The value of τ_p is determined by computing the location of the dominant peak in the cross-correlation function, which corresponds to the point in time where the two signals are best aligned [Yang et al. (2022)]. Since the spacing between the two transducers is already known, the particle velocity is calculated as shown in (7).

$$v = \frac{L}{\tau_p} \tag{7}$$

where, L is the distance between upstream and downstream electrodes and τ_p is the time that solid particles take to move from upstream to downstream transducer electrodes.

C. Electrostatic Sensor Setup

In this research, electrostatic sensors are used as transducers to acquire the correlated signals. The electrostatic sensor is a passive device that measures the charge value of the solid particles. Hence, first, the charge signals are converted into corresponding voltage signals [Qian et al. (2017)]. These voltage signals are amplified to ensure their accurate recognition and interpretation by the acquisition system. The final stage of the conditioning circuit comprises a low pass filter that removes the high-frequency noise to remove unnecessary chattering content from the signal. The sensor layout is shown in Figure 1 (a). The two ring-shaped electrostatic electrodes are flush mounted with the walls of the sensing head [Yan (2005)]. In this work, the value of L is set at 16 mm. the disturbance in the gas-solid flow is introduced using a rectangular shape strip as shown in Figure 1 (b).

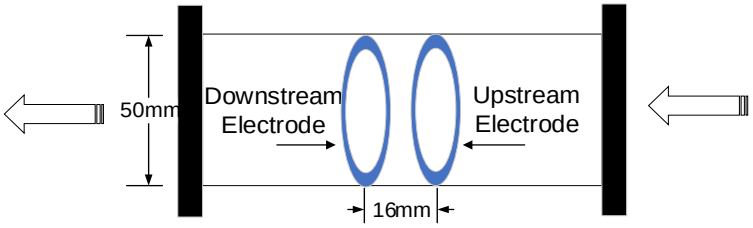

(a)

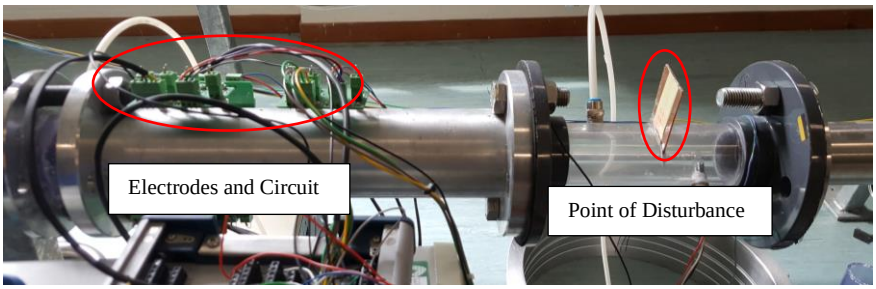

(b)

Figure 1. (a) Layout of sensor design (b) Sensing head with source of disturbance.

III. Proposed Control Methodology

The proposed control scheme works by dynamically updating the fractional orders based on the real-time error variations in the velocity of solid particles. The overall closed-loop system, along with the proposed methodology, is shown in Figure 2 (a). The whole process starts with a velocity setpoint v_{set} prescribed by the user. The difference between v_{set} and the particle's actual velocity v_o yields the velocity error $e(t)$. The values of $e(t)$ and its derivative, $\dot{e}(t)$, are fed to pre-calibrated hyperbolic secant functions (HSFs) that modify the fractional orders online. The PID gains and the variation rates of the HSFs are pre-calibrated offline by using the GA. The AFOPID controller uses the error variations to generate a voltage signal that is bounded within 0

- 10 V. The variable frequency drive (VFD) uses this voltage to vary the pump's frequency between 0 - 50 Hz to control its suction power. The schematic of the test rig used for this purpose is shown in Figure 2 (b).

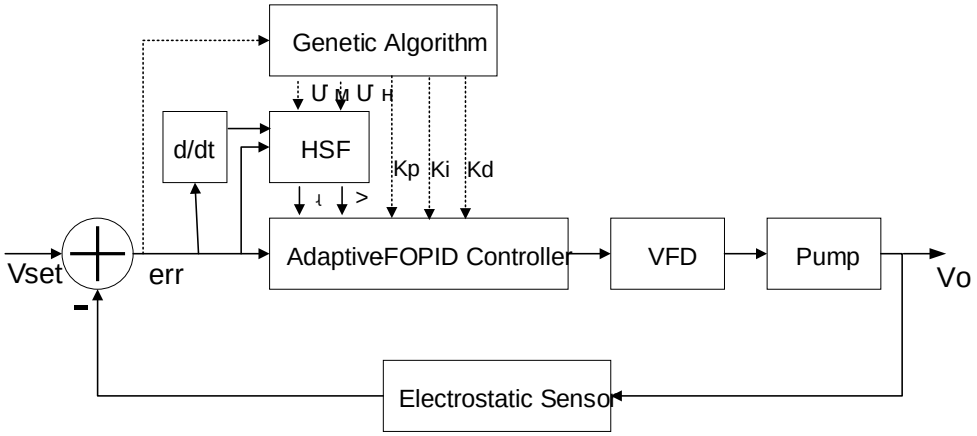

(a)

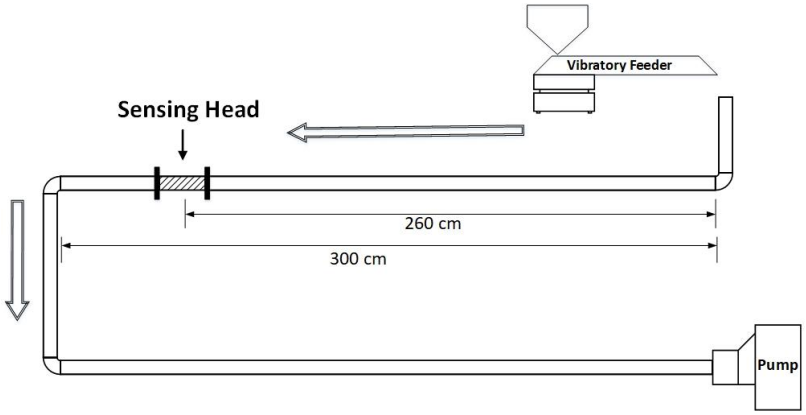

(b)

Figure 2. (a) AFOPID control algorithm (b) Test rig schematic.

A. Integer Order PID Controller

The conventional PID controller is formulated as the weighted sum of the classical error variable, the integer-order error-integral variable, and the integer-order error-derivative variable. The linear combination of the aforesaid error variables is expressed as shown in (8).

$$u(t) = k_p e(t) + k_i \int_o^t e(\tau)\, d\tau + k_d \dot{e}(t) \tag{8}$$

such that, $e(t) = v_{set} - v_o$

where, k_p, k_i and k_d are the proportional, integral, and differential gains, respectively. The proportional controller improves the reference-tracking accuracy of the closed-loop system. The integral controller attenuates the overshoots and minimizes the steady-state fluctuations. The derivative controller enhances the phase margin and the response speed of the system [Shang et al. (2009)]. Altogether, these terms increase the controller's agility to flexibly manipulate the stiffness of the control input as the error conditions vary [Saleem et al. (2020)]. The PID gains are optimized offline via GA discussed in Section IV.

B. Fractional Order PID Controller

Despite its reliability, the integer-order PID controller lacks the robustness to compensate for nonlinear disturbances [20]. This problem can be addressed by retrofitting the integer-order PID control law with fractional calculus.

Fractional calculus serves as an effective tool to realize and reject intrinsic and unmodeled nonlinear disturbances. The fractional control law is realized by replacing the integer-order integral and differential operators with their fractional-order counterparts. This augmentation increases the controller's flexibility, which enhances its resilience against exogenous disturbances. To implement the fractional control law, integral and

differential operators are assigned fractional number powers. In this article, the fractional operators are denoted as D^{ε}, where ε is the fractional order. The three well-known definitions governing fractional calculus are given by Riemann-Liouville, Gruunwald-Letnikov, and Caputo [24]. These definitions are expressed as follows, respectively.

$$D^{\varepsilon}f(t) = \frac{1}{\Gamma(n-\varepsilon)}\frac{d^n}{dt^n}\int_a^t \frac{f(\tau)}{(t-\tau)^{\varepsilon-n+1}}d\tau \tag{9}$$

where, $f(t)$ is an arbitrary function, $\Gamma(.)$ is the Euler gamma function, n is an integer number, and $n-1 < \varepsilon < n$.

$$D^{\varepsilon}f(t) = \lim_{h\to 0}\frac{1}{h^{\varepsilon}}\sum_{j=0}^{(t-a)/h}(-1)^j\binom{\varepsilon}{j}f(t-jh) \tag{10}$$

where, $\binom{\varepsilon}{j} = \Gamma(\varepsilon+1)/\Gamma(j+1)\,\Gamma(\varepsilon-j+1)$, and h is the step size.

$$D^{\varepsilon}f(t) = \frac{1}{\Gamma(\varepsilon-n)}\int_a^t \frac{f^n(\tau)}{(t-\tau)^{\varepsilon-n+1}}d\tau \tag{11}$$

The integer-order PID control law, designed in the previous subsection, is retrofitted with fractional order integral and derivative operators to realize the FOPID control law. The fractional powers of the integral and derivative operators, δ and μ, are treated as the two new hyper-parameters. The FOPID control law is formulated as shown in (12).

$$u(t) = k_p e(t) + k_i\left(D^{-\delta}e(t)\right) + k_d(D^{\mu}e(t)) \tag{12}$$

where, k_p, k_i and k_d are the same proportional, integral, and differential gains as prescribed in the last sub-section. The fractional orders δ and μ are meta-heuristically tuned via the GA. The offline tuning procedure is discussed later in this article. The transfer functions of the control laws $u(t)$ is presented in (13).

$$C(s) = \frac{U(s)}{E(s)} = k_p + k_d s^{\mu} + \frac{k_i}{s^{\delta}} \tag{13}$$

It is quite difficult to computationally realize the terms s^{δ} and s^{μ} due to their fractional nature. Hence, these fractional operators are digitally implemented by using the Oustaloup recursive filtering technique [27]. The fractional operator s^{ε} is approximated via the Oustaloup filter, as shown in (14).

$$s^{\varepsilon} = P \prod_{i=1}^{M} \frac{1 + \left({}^{s}/_{\omega_{z,i}}\right)}{1 + \left({}^{s}/_{\omega_{p,i}}\right)} \tag{14}$$

such that, $\omega_{z,i} = \omega_l \left({}^{\omega_h}/_{\omega_l}\right)^{{}^{2i-1-\varepsilon}/_{2M}}, \omega_{p,i} = \omega_l \left({}^{\omega_h}/_{\omega_l}\right)^{{}^{2i-1+\varepsilon}/_{2M}}$

where, ω_h and ω_l are the upper and the lower translational frequencies of the filter, respectively, and M is the filter order. The value of P is selected such that $(j\omega)^{\varepsilon} = 1$ at 1.0 rad/s. In this research, a fifth order Oustaloup's recursive filter is employed with $\omega_l = 10^{-4}$ rad/s and $\omega_h = 10^{2}$ rad/s to realize the fractional operators. The stability and robustness of the designed FOPID controller are analyzed as per the basic definitions of the gain margin and phase margin in the frequency domain. The feedback control system is required to satisfy the following conditions to ensure its stability [Hui et al. (2019)].

- The phase of the open loop at the gain cross-over frequency ω_c satisfies: $arg\big(C(j\omega_c)G(j\omega_c)\big) = \varphi_m - \pi$, where φ_m is the phase margin.
- The gain of the open loop at ω_c satisfies: $|C(j\omega_c)G(j\omega_c)| = 0\ dB$
- To ensure robustness against loop gain variations, the phase satisfies: $\frac{d}{d\omega}\left[arg\big(C(j\omega)G(j\omega)\big)\right]|_{\omega=\omega_c} = 0$.
- To attenuate high-frequency noise $\omega \geq \omega_h$, the magnitude of the closed-loop transfer function Q must satisfy: $\left|Q(j\omega_h) = \frac{C(j\omega_h)G(j\omega_h)}{1+C(j\omega_h)G(j\omega_h)}\right| < H\ dB$.

- To attenuate low-frequency noise $\omega \leq \omega_l$, the sensitivity function S satisfies: $\left|S(j\omega_l) = \frac{1}{1+C(j\omega_l)G(j\omega_l)}\right| \leq M\ dB$.

For the setup uses in this work, the following specifications can be considered; $\varphi_m = 0.785\ rad.$, $\omega_c = 0.5$, $H = -10$, and $M = -20$. These specifications can be used to compute the five parameters of the FOPID controller while preserving its asymptotic stability. Since it is quite hard to evaluate the analytical solutions, GA is used in this work to optimize the said parameters. The GA-based offline tuning of the FOPID controller parameters is discussed in Section IV.

C. Adaptive Fractional Order PID Controller

Despite the optimum tuning of the fractional orders, the consequent FO-PID controller would still lack the adaptability to flexibly manipulate the stiffness of the control effort to robustly compensate for the bounded exogenous disturbances, load-step variations, and measurement noise. This is because assigning a unique set of preset values to the controller gains and fractional orders is insufficient to address and yield the best control behavior against every disturbance condition.

The aforementioned problem can be easily addressed by retrofitting the FO-PID controller with an online adaptation mechanism that dynamically modulates the fractional orders δ and μ as a nonlinear function of state error variables [26]. It is well-known that an appropriate setting of δ and μ can transform the FO-PID controller into its integer-order variants; the P, PI, PD, and PID controllers. Each of these controller subclasses exhibits beneficial features to handle the response as it commutes between its different phases.

Hence, in this work, the proposed adaptation mechanism acts as a superior regulator to adaptively modulate the fractional orders so that the FO-PID controller can be smoothly transformed into its appropriate subclasses as the error conditions vary. The adaptation mechanism is formulated by using the following meta-rules [27].

- The value of μ is increased during the initial start-up as well as the transient disturbances, and vice versa, to strengthen the derivative action. This arrangement increases the system's response speed and tightens the control application.
- The value of δ is increased during steady state conditions, and vice versa, to strengthen the integral action. This improves the system's damping against steady-state fluctuations, allowing it to settle smoothly at the set point.

These rules tend to increase the system's response speed while strengthening its damping effort against overshoots. The arrangement enables the controller to satisfy the desired objectives while addressing the disturbances. The AFOPID controller is formulated as per the aforementioned meta-rules. The fractional orders are dynamically adjusted as a nonlinear function of the classical error and its derivative. The AFOPID control law is formulated as shown in (15).

$$u(t) = k_p e(t) + k_i \left(D^{-\delta(z,t)} e(t)\right) + k_d \left(D^{\mu(z,t)} e(t)\right) \tag{15}$$

where, k_p, k_i and k_d are the proportional, integral, and differential gains, respectively. The fractional orders δ and μ are dynamically modified via the hyperbolic secant functions (HSFs) shown in (16) and (17).

$$\delta(z,t) = \operatorname{sech}\left(\gamma_1 z(t)\right) \tag{16}$$

$$\mu(z,t) = 1 - \operatorname{sech}\left(\gamma_2 z(t)\right) \tag{17}$$

where, γ_1 and γ_2 depict the variation rates of the HSF $\operatorname{sech}(.)$, and $z(t)$ is the maximum value chosen between the normalized value of classical error $\hat{e}(t)$ and derivative of normalized errors $\hat{\dot{e}}(t)$. The HSFs are chosen in

this work because they are continuous, even-symmetric, and bounded between zero and unity. These features lead to smooth transitions of δ and μ while restricting them between zero and unity, irrespective of the sign of $z(t)$. The variable $z(t)$ is expressed as shown in (18).

$$z(t) = \max\left(\hat{e}, \hat{\dot{e}}\right) \tag{18}$$

The particle velocity is estimated via the cross-correlation technique, which is then used to compute $e(t)$. Numerical differentiation of $e(t)$ delivers $\dot{e}(t)$. The instantaneous values of $e(t)$ and $\dot{e}(t)$ are normalized, as shown in (19).

$$\hat{e}(t) = \left|\frac{e(t)}{e_{max}}\right| = \left|\frac{e(t)}{v_{set}}\right|, \qquad \hat{\dot{e}}(t) = \left|\frac{\dot{e}(t)}{\dot{e}_{max}}\right| \tag{19}$$

The maximum error occurs when the particle's velocity is zero. In this case, the error becomes equal to the reference velocity. The maximum value of the derivative of error is determined experimentally to be 12 m/s for this research work. To ensure the system's stability with the proposed methodology, all the controller gains and the other parameters need to be kept within the range described in Table I. The parameter adaptation procedure does not put any recursive computational burden on the computer. Hence, the scheme can be easily realized with modern digital computers. The proposed control guarantees asymptotic convergence if the conditions prescribed in the previous sub-section are satisfied. The parameters k_p, k_i, k_d, γ_1, and γ_2 are tuned offline via the GA as discussed in Section IV.

IV. Parameter Optimization

The GA is a heuristic search and optimization algorithm that is inspired by the theory of natural evolution by Charles Darwin. The GA technique offers several advantages over other optimization schemes [Lazarevic et al. (2013)].

Table I. Range of Controller parameters

Parameters	Min.	Max.
k_p	0.01	1
k_i	1	10
k_d	0.001	0.1
δ	0.1	1
μ	0.1	1
γ_1	0.01	1
γ_2	1	20

The GA is a stochastic search method that imitates the evolution processes observed in nature [Guo et al. (2010)]. It can afford parallelism to solve optimization tasks. It is simple, requires less information, offers a higher convergence rate, and can handle larger sets of solution spaces as compared to other techniques [Guo et al. (2010)]. It represents natural genetics using chromosomes to perform parameter optimization and can be applied to a vast variety of practical engineering problems. These features make GA the ideal candidate to optimize the controller parameters for this work. This algorithm uses the natural selection process in which the most suitable people are chosen for reproduction to generate the next generation of children. The algorithm contains five steps that are described as follows:

1) ***Initialization:*** The method starts with a collection of random parameters denoted as the 'population'. Every parameter in the population is a candidate solution to the optimization problem. The population is chosen such that the algorithm yields faster convergence while preserving the quality of the solutions as well as the computational economy. For this purpose, different population sizes (e.g., 50, 100, 200) were analyzed, and

the algorithm's corresponding performance in terms of convergence speed and quality of solutions was observed. Consequently, a population size of 100 is selected for this application.

2) ***Evaluation:*** The likelihood of selecting a parameter for reproduction is based on its fitness value. Every parameter is assigned a fitness value. The percentage overshoot (PO), settling time (t_s), rise time (t_r), and summation of all steady-state errors (e_{ss}) are used to ascertain the fitness of the parameter. The fitness function is shown in (20).

$$J_f = |PO| + t_s + t_r + \int_0^\infty |e_{ss}(t)|dt \tag{20}$$

The computation of the solutions to the optimization problem is directly impacted by the selection of the weighting factors of the performance indices in the cost function. Applying a higher weighting factor to t_s and t_r allows the controller to respond more quickly to changes in the system, leading to a faster transient response, and better tracking of desired references. However, it also contributes to larger overshoots and steady state fluctuations. On the contrary, applying a higher weighting factor to PO or integral of e_{ss} reduces the overshoots and potentially attenuates the steady-state fluctuations. However, it also slows the response speed and prevents the controller from keeping up with rapid changes in the system, leading to poor tracking performance.

Imposing equal weights on each performance index typically establishes a beneficial trade-off between the system's tracking performance, robustness against disturbances, and transient speed. By setting all weights to unity, each performance index is considered equally important. This approach assumes that all parameters have the same impact on the overall cost, thus simplifying the optimization problem. In the absence of specific knowledge about the relative importance of different performance indices, setting all weights to

unity is a neutral starting point. This avoids the introduction of bias that might come from arbitrary weighting. Hence, in this research, a weighting factor of 1 is applied to each performance metric in J_f.

3) ***Selection:*** This stage selects the fittest parameters and transfers their properties to the next generation. The number of iterations (or generations) is determined based on empirical testing with various numbers of generations (e.g., 50, 100, 200) via pilot algorithmic runs until improvements in fitness are negligible (convergence). The algorithm is thus run for 50 iterations in this research because the entire system takes considerable time to converge to the reference velocity. The chosen number of iterations yielded near-optimal solutions while preserving the computational economy.
4) ***Crossover:*** Two previously existing parameters exchange their properties to reproduce the next generation of parameters that can be added to the population. The new parameters are generated as shown in (21) and (22).

$$Y_1 = |\beta_1 X_1 + (1 - \beta_2) X_2| \tag{21}$$

$$Y_2 = |(1 - \beta_1) X_1 - \beta_2 X_2| \tag{22}$$

where, β_1 and β_2 are crossover rates that are bounded between 0 and 1, X_1 and X_2 are the parent elements that contribute their properties to generate new parameters Y_1 and Y_2. Generally, a higher crossover rate promotes exploration but can disrupt good solutions, whereas, a lower crossover rate promotes exploitation but can lead to premature convergence. By conducting preliminary runs of the algorithm, $\beta_1 = 0.4$ and $\beta_2 = 0.6$ is selected. This set of empirically selected crossover rates balances exploration and exploitation for this application.

5) ***Mutation:*** Mutation happens within the population to preserve diversity and damp premature convergence by flipping some of the bits within one parameter.

The inner parameters of the GA are empirically tuned via the following steps: An initial set of inner parameters (populations, generations, and crossover rates) is chosen based on literature and general guidelines. A few pilot runs of the algorithm are then performed to understand the GA's behavior. One inner parameter is adjusted at a time, and its impact on the GA's performance is observed. This process of refining the inner parameters and testing the algorithm until its performance is satisfactory. That is, the algorithm's convergence rate improves while preserving the quality of the solutions as well as the computational budget.

The algorithm's flow is illustrated in Figure 3. The controller parameters ($k_p, k_i, k_d, \delta, \mu, \gamma_1,$ and γ_2) of the PI, PID, FOPI, FOPID, and AFOPID controllers are optimized offline via GA to ensure a fair comparison between the three control variants. While optimizing a particular controller variant, the GA chooses the random initial value of the parameters from the selection ranges (identified in Table I) and evaluates their fitness J_f by running the conveying system to track the 20 m/s velocity set point for 40 sec. The optimized controller parameters are recorded in Table II.

V. Experimental Analysis

This section describes the experimental procedure and analyzes the experimental outcomes.

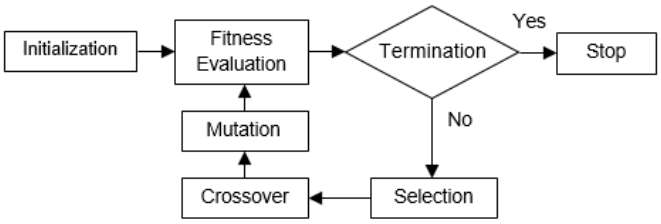

Figure 3. Flow chart of GA.

Table II. Selected control parameters

Controller	k_p	k_i	k_d	δ	μ	γ_1	γ_2
PI	0.50	5.1	-	-	-	-	-
PID	0.50	5.0	4.9×10^{-3}	-	-	-	-
FOPI	0.52	3.1	3.4×10^{-3}	0.85	-	-	-
FOPID	0.52	3.2	3.4×10^{-3}	0.92	0.181	-	-
AFOPID	0.48	2.1	4.8×10^{-3}	HSF	HSF	0.05	10

A. Experimental Setup

All experiments are conducted on a laboratory-scale negative pressure test rig, as shown in Figure 4 (a). In this research, the velocity of pneumatic conveyance of fine whole-grain wheat flour particles is used to analyze the performance of the proposed control scheme in the physical environment. The flour particles are placed in the vibratory feeder that conveys them to the pipe inlet of 0.05 m diameter. A suction pump is installed at the pipe's other end to move these particles at the desired velocity. Hence, a VFD is commissioned to control the pump's suction power via a personal computer (PC). A separate sensing head is installed at 2.6 m from the starting point of the horizontal pipe to analyze the behavior of the charge absorbed by the solid particles. The measurements are acquired via the NI-DAQ card at a sampling rate of 50 kHz. The acquired signals are conditioned and serially transferred to the software control routine running on the PC. The DAQ card also receives control commands from the PC and applies them to the VFD, as shown in Figure 4 (b).

The proposed control system is programmed in the Windows-based MATLAB application using the FOMCON toolbox. The toolbox uses the Oustaloup recursive approximation to approximate fractional-order operators in the continuous domain. This involves generating a continuous-time rational transfer function with a specified number of poles and zeros to approximate the fractional order over a given frequency range.

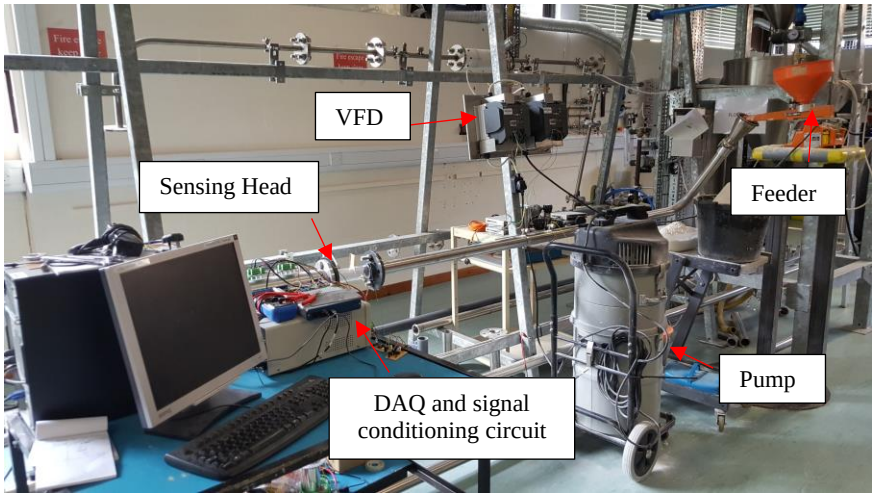

(a)

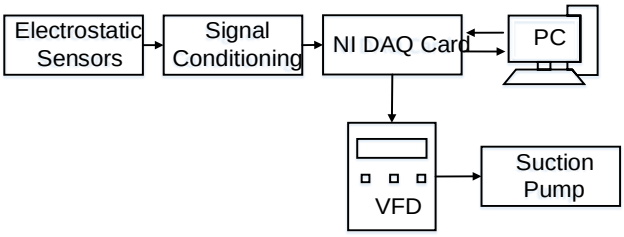

(b)

Figure 4. (a) Laboratory scale test rig, (b) Data acquisition and control system.

For implementation in digital controllers, FOMCON provides built-in functions to discretize the continuous-time approximation. This is typically done using methods like the Tustin (bilinear) transformation or other discrete approximation techniques, allowing the continuous-time model to be used in discrete-time systems.

The Oustaloup filter provides a rational function approximation that can be applied in the continuous domain, which can then be discretized for implementation in digital systems.

The implementation of the proposed control algorithm involves a higher computational burden compared to simpler control algorithms like the traditional PID controller. This increased computational complexity arises from the need to approximate fractional order integrals and derivatives, which inevitably increases the memory requirements as well as the complexity and the number of calculations per sampling interval. However, the said computational load can be easily handled with modern day programmable-logical-controllers (PLCs) or digital controllers; given that these systems support a high-level programming language (such as, structured text and function block diagrams), a sufficient sampling rate (at least 50 kHz), an adequate memory, and processing power. Hence, the proposed scheme can be practically integrated into industrial applications.

B. Tests and Results

Two unique experimental scenarios are used to assess the real time performance of the proposed control scheme. In every experimental trial, irrespective of the controller variant being used or the test condition being applied, the system starts with the vibratory feeder supplying the same (preset) quantity of solid particles while the pump's VFD adjusts the suction power to meet the desired set point. The details of the two experimental tests, the corresponding results, and the performance analysis are presented as follows:

1. Tests under Different Velocity Set Points

The reference-tracking behavior of each control scheme is tested with three different velocity set points for a duration of 40 sec. to analyze their performance. The variation in velocity set points is a common occurrence in practical conveying systems and this test case emulates the aforementioned phenomenon. The minimum

velocity required to drive the particles in the pneumatic pipeline of the hardware setup used in this work is 15 m/s. Below this threshold, the particles tend to accumulate at the bottom of the pipe.

The air velocity measurement capability of the hot anemometer used in this work is limited to 26 m/s. In compliance with the aforementioned constraints, the three equally spaced velocity set-points are chosen from the range of 15 m/s to 25 m/s. Hence, the test results for 15 m/s, 20 m/s, and 25 m/s velocity set points are illustrated in Figure 5(a) to 5(c) respectively. The performance of AFOPID is compared with classical PI, PID, FOPI, and FOPID controllers. The AFOPID outperforms the other control techniques in terms of rise time (t_r), settling time (t_s), percentage overshoot (PO), steady-state error (e_{ss}), integral square-of-error (ISE), and integral time-weighted absolute error (ITAE) as shown in

Table III. The PI and FOPI controllers minimize the chattering content but also slow down the response. The PID exhibits faster transition at the cost of large overshoots and chattering. The FOPID controller exhibits a mediocre improvement in time-domain performance. The AFOPID controller yields the most time-optimal behavior with minimal fluctuations.

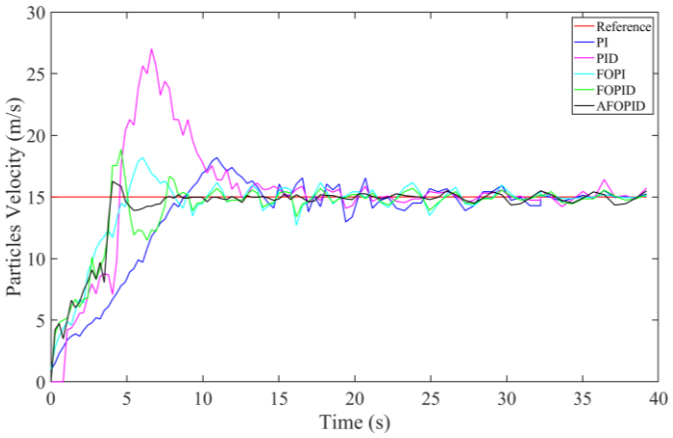
Reference
PI
PID
FOPI
FOPID
AFOPID
Particles Velocity (m/s)
Time (s)
0
5
10
15
20
25
30
35
40

(a)

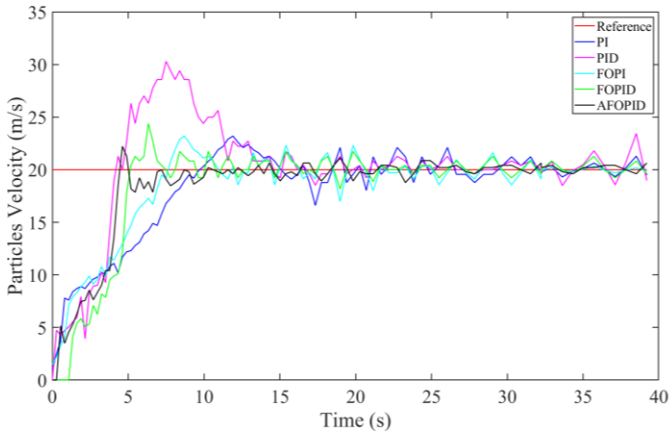
Reference
PI
PID
FOPI
FOPID
AFOPID
Particles Velocity (m/s)
Time (s)
0
5
10
15
20
25
30
35
40

(b)

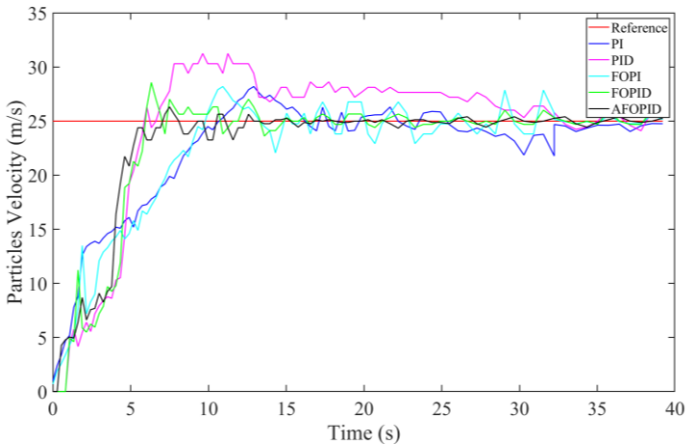

(c)

Figure 5. Response of the controllers with velocity set point (a) 15 m/s (a) 20 m/s (a) 25 m/s

Table III. Experimental Result Summary under Different Velocity Set Points

Velocity (m/s)	**Controller**	t_r **(s)**	t_s **(s)**	PO **(%)**	e_{ss} **(m/s)**	**ISE** $(m/s)^2$	**ITAE (m)**
15	PI	8.56	27.55	23.17	0.41	4.21×10^3	42.23
	PID	4.62	21.15	80.18	0.48	2.90×10^3	33.29
	FOPI	6.72	20.18	22.88	0.33	1.89×10^3	20.21
	FOPID	4.16	18.15	25.79	0.38	1.25×10^3	18.30
	AFOPID	4.05	7.50	8.46	0.27	0.98×10^3	13.61
20	PI	9.38	35.33	20.12	0.33	5.12×10^3	45.87
	PID	4.33	34.32	51.52	0.37	4.92×10^3	39.01

	FOPI	7.51	33.95	21.18	0.28	4.14×10^3	32.33
	FOPID	5.18	33.63	21.95	0.29	3.20×10^3	31.92
	AFOPID	4.62	10.28	11.11	0.23	2.91×10^3	26.23
25	PI	9.18	37.25	14.56	0.47	8.65×10^3	63.25
	PID	5.77	36.84	25.00	0.56	7.60×10^3	55.44
	FOPI	8.26	31.89	14.23	0.51	7.23×10^3	40.02
	FOPID	5.77	23.55	14.29	0.46	6.63×10^3	39.36
	AFOPID	6.93	12.64	5.26	0.24	5.62×10^3	29.87

2. Tests under Different Disturbance Levels

The second set of experiments is done with three different disturbance levels. The disturbances are injected into the system by blocking a portion of the pipe with a rectangular strip of three different sizes, as shown in Figure 1. This practical disturbance scenario is designed specifically to emulate different levels of blockage that occur in the conveying system in real time. Three different disturbance levels (L1, L2, and L3) are chosen that block 25%, 50%, and 75% of the cross-section area of the pipe, respectively. The aforementioned blockage percentages are chosen to analyze the system at three different (equally spaced) blockage levels. This test assesses the system's robustness as the disturbance levels are systematically increased by a 25% step in each case. The test results are illustrated in Figure 6(a) to 6(c), respectively. In each case, the disturbance is introduced during steady-state conditions. Each controller is analyzed based on its transient-recovery time (t_{rec}), mean absolute error (MAE), ISE, and ITAE.

The experimental results are summarized in Table IV. The introduction of a bounded disturbance in continuous flow causes a sudden fall in velocity, as shown in Figure 6 (a). However, the sudden rise in velocity in Figure 6 (b) and Figure 6 (c) at the time of disturbance application is caused by the incremental blockage level, which

enables the particles lying at the bottom of the pipe to flow with higher air pressure and a higher velocity. The PI controller and the FOPI controller exhibit fragile damping against disturbance-induced undershoots, along with a slow transient recovery. The PID exhibits a relatively quicker transient recovery behavior while contributing a large undershoot. The FOPID controller exhibits a reasonable improvement in damping control activity and response speed. The AFOPID controller exhibits rapid transits with relatively stronger damping against undershoots.

The system learns about the disturbances by observing the variations in the state error dynamics, namely, the error, error derivative, and integral of error. Together, these three state variables provide the closed-loop system with an accurate estimate regarding the magnitude of disturbance encountered by it. The customized state observers are not used to avoid additional computational load, noise sensitivity, and implementation complexity [Yuan and Gao (2019)].

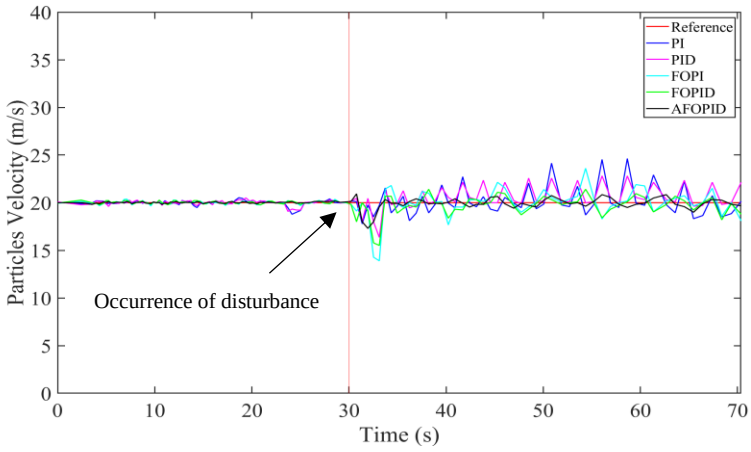

(a)

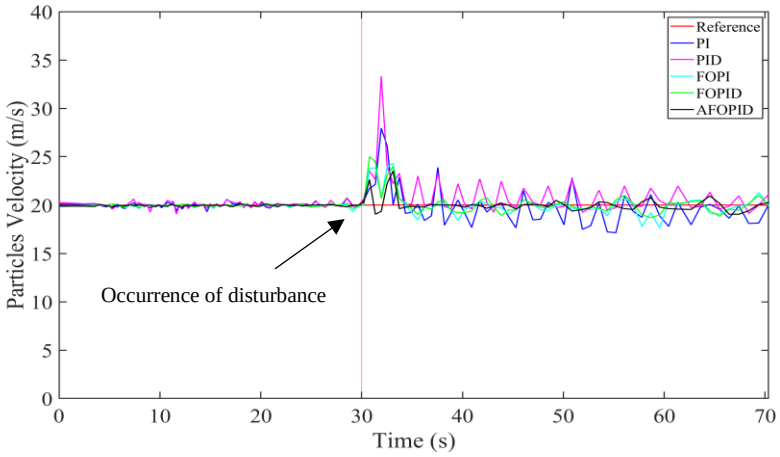

(b)

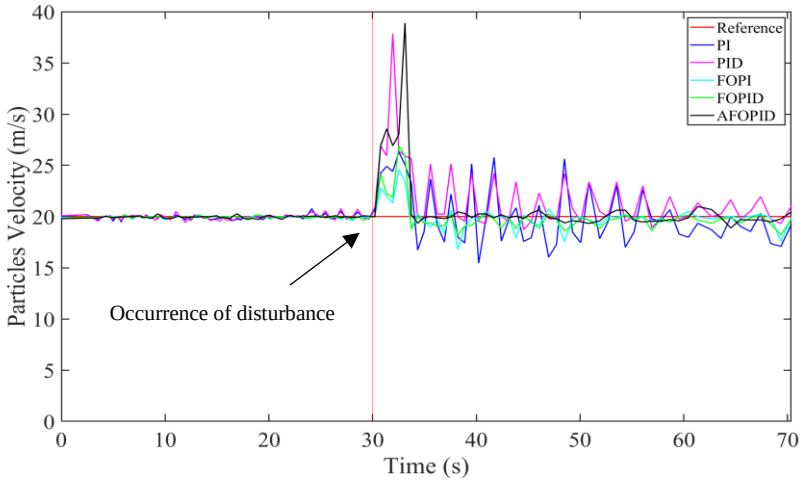

(c)

Figure 6. Response of the controllers upon disturbance level (a) L1 (b) L2 (c) L3

VI. CONCLUSION

This article systematically formulates an innovative self-adaptive FOPID control scheme for particle velocity regulation in an industrial pneumatic conveying system to enhance its time optimality, adaptability, and robustness against bounded disturbances. The innovative adaptive tuning of fractional orders using error-driven scaling functions has enhanced the flexibility of the proposed control law to achieve the desired control objectives. Three control algorithms are implemented and investigated to regulate the velocity of pneumatically conveyed solid particles. Reliable hardware experiments are conducted to analyze the efficacy of the AFOPID control law. The AFOPID controller surpasses all the other controller variants by displaying enhanced time-domain performance and superior disturbance-compensation capability.

Table IV. Experimental result summary under different disturbance levels

Disturbance	**Controller**	t_{rec} **(s)**	**MAE (m/s)**	**ISE (m/s)^2**	**ITAE (m)**
L1	PI	40.23	0.56	105.21	5.12
	PID	38.17	0.48	99.96	4.93
	FOPI	36.47	0.42	72.58	4.23
	FOPID	10.70	0.38	69.76	3.91
	AFOPID	2.91	0.27	23.32	2.23
L2	PI	40.74	0.51	350.57	7.89
	PID	35.26	0.37	302.75	6.83
	FOPI	33.82	0.33	88.13	5.14
	FOPID	4.45	0.26	87.81	4.09
	AFOPID	3.52	0.16	32.35	2.33
L3	PI	35.83	0.57	700.21	12.18
	PID	26.71	0.56	684.48	10.62

	FOPI	21.66	0.49	145.29	6.65
	FOPID	8.67	0.46	133.86	4.69
	AFOPID	3.52	0.24	31.25	2.58

It exhibits rapid transits with strong damping against overshoots and steady-state fluctuations while tracking the velocity set points: 15 m/s, 20 m/s, and 25 m/s. Under different disturbance levels, when the cross-section area of the pipe was blocked systematically, it was observed that the AFOPID accurately tracks the set point velocity and quickly converges to the setpoint, effectively rejecting the overshoot. It exhibits the strongest immunity against bounded exogenous disturbances and improves the transient recovery time by 10 folds as compared to the conventional control schemes analyzed in this research. Similarly, it also improves the MAE, ISE, and ITAE metrics by at least two times. The study shows that the FOPID controller for the pneumatic conveying system demonstrates superior agility and robustness as compared to the other controllers due to the introduction of the two self-adjusting parameters that increase the controller's design flexibility. Thus, it is concluded that the AFOPID controller performs better than other classical control schemes by effectively rejecting disturbances.

There is still a lot of room for future enhancements. The proposed scheme can be investigated with other meta-heuristic optimization algorithms. Other expert adaptation systems can be assessed to improve the control yield of the proposed scheme. With the specialized hardware setup and data acquisition of the appropriate state variables, the proposed scheme has the potential to be applied to networked control applications as well. Furthermore, the proposed scheme can be modified to control the behavior of under-actuated mechatronic systems, renewable energy conversion systems, robotic manipulators, aircraft control, satellite attitude and orbital control, humanoid robot control, and biological systems (such as glycemic regulators). Finally, the

transient response speed and reference tracking accuracy of the proposed AFOPID controller can be experimentally compared with those of the adaptive PID controller whose integral and differential gains are dynamically adjusted online using pre-calibrated adaptation functions, customized to address the requirements of pneumatic conveying systems.

REFERENCES

[Abe el al. (2023)] Abe, M.C., Gelladuga, G.A., Mendoza, C.J., Natavio, J.M., Zabala. J.S., & Lopez E.C.R. (2023), 'Pneumatic Conveying Technology: Recent Advances and Future Outlook,' *Engineering Proceedings* **56(1)**, 205.

[Barbosa & Seleghim (2003)] Barbosa, P.R. & Seleghim, P. (2003), 'Improving the power consumption in pneumatic conveying systems by adaptive control of the flow regime', *Journal of the Brazilian society of mechanical sciences and engineering* **25**, 373-377.

[Barbosa & Seleghim (2011)] Barbosa, P. R. & Seleghim, P. (2011), 'On the application of fuzzy logic control in pneumatic conveying systems', *Learning and Nonlinear Models* **9**, 256–265.

[Barratt et al. (2000)] Barratt, I., Yan, Y., Byrne, B. & Bradley, M. (2000), 'Mass flow measurement of pneumatically conveyed solids using radiometric sensors', *Flow Measurement and Instrumentation* **11**(3), 223–235.

[Bequette (2003)] Bequette, B., W. (2003), *Process Control: Modeling, Design, and Simulation*, 1st edn, Prentice Hall, New Jersey.

[Birk (1999)] Birk, W. (1999), Multivariable control of a pneumatic conveying system, Dissertation, Lulea University of technology.

[Coombes & Yan (2016)] Coombes, R. J. & Yan, Y. (2016), 'Measurement of velocity and concentration profiles of pneumatically conveyed particles using an electrostatic sensor array', *IEEE Transaction on Instrumentation and Measurement* **65**(5), 1139–1148.

[Deloughry et al. (2001)]Deloughry, R., Pickup, E. & Ponnapalli, P. (2001), 'Closed loop control of a pneumatic conveying system using tomographic imaging', *Journal of Electronic Imaging* **10**.

[Dumlu & Erenturk (2014)] Dumlu, A. & Erenturk, K. (2014), 'Trajectory tracking control for a 3-dof parallel manipulator using fractional-order $PI^{\lambda}D^{\mu}$ control', *IEEE Transactions on Industrial Electronics* **61**(7), 3417–3426.

[Erenturk (2013)] Erenturk, K. (2013), 'Fractional-order pid and active disturbance rejection control of nonlinear two-mass drive system', *IEEE Transactions on Industrial Electronics* **60**(9), 3806–3813.

[Genxi et al. (2008)] Genxi, G., Baolu, Z., Liangyun, W., Yu, H., Xiaohua, H., Qiyou, T. (2008), 'Design of automatic control system with remote pneumatic conveying feeding system based on PLC,' *South China Fisheries Science* **4(6)**, 7-16.

[Giernacki (2016)] Giernacki, W. (2016), Near to optimal design of pid fractional-order speed controller (fopid) for multirotor motor-rotor simplified model, *in* '2016 International Conference on Unmanned Aircraft Systems (ICUAS)', Arlington, VA, pp. 320–326.

[Guo et al. (2010)] Guo, P., Wang, X. & Han, Y. (2010), The enhanced genetic algorithms for the optimization design, *in* '2010 3rd International Conference on Biomedical Engineering and Informatics', Vol. 7, Yantai, China, pp. 2990–2994.

[Hui et al. (2019)] Hui, P., Ping, W. & Weihua, L. (2019), Model based fractional order PID controller design and simulation of pressure swing adsorption, *in* 'Chinese Control Conference (CCC)', pp. 2880–2883.

Jones, M.G. & Jacob, M. (2007), 'Advances in Pneumatic Conveying Using Model Predictive Control', *Powder Technology* **179(3)**, 195-202.

[Klinzing et al. (2010)] Klinzing, G. E., Marcus, R. D., Rizk, F., & Leung, L. S. (2010), 'Pneumatic Conveying of Solids: A Theoretical and Practical Approach,' Springer: Berlin.

[Lazarevic et al. (2013)] Lazarevic, M. P., Batalov, S. A. & Latinovic, T. S. (2013), 'Fractional pid controller tuned by genetic algorithms for a three dof's robot system driven by dc motors', *IFAC Proceedings Volumes* **46**(1), 385 – 390. 6th IFAC Workshop on Fractional Differentiation and Its Applications.

[Mills (2004)] Mills, D. (2004), 'Pneumatic Conveying Design Guide,' Butterworth-Heinemann.

[Mishra & Chandra (2014)]Mishra, Kumar, S. & Chandra, D. (2014), 'Stabilization and tracking control of inverted pendulum using fractional order pid controllers', *Journal of Engineering* **2014**, 1–9.

[Neuffer et al. (1999)] Neuffer, D., Alvarez, A., Owens, D., Ostrowski, K., Luke, S. & Williams, R. (1999), 'Control of pneumatic conveying using ect', *1st World Congress on Industrial Process Tomography Buxton, Greater Manchester* .

[Penirschke et al. (2008)] Penirschke, A., Rijiranuwa, A., Maune, H., Schubler, M. & Jakoby, R. (2008), Microwave mass flow sensor for process monitoring applications, *in* '2008 IEEE MTT-S International Microwave Symposium Digest', Atlanta, GA, USA, pp. 1195–1198.

[Qian et al. (2017)] Qian, X., Yan, Y., Huang, X. & Hu, Y. (2017), 'Measurement of the mass flow and velocity distributions of pulverized fuel in primary air pipes using electrostatic sensing techniques', *IEEE Transactions on Instrumentation and Measurement* **66**(5), 944–952.

[Qian et al. (2015)] Qian, X., Yan, Y., Wang, L. & Shao, J. (2015), 'An integrated multi-channel electrostatic sensing and digital imaging system for the on-line measurement of biomass-coal particles in fuel injection pipelines', *Fuel* **151**, 2–10.

[Ren, Fan & Kaynak (2019)] Ren, H.-P., Fan, J.-T. & Kaynak, O. (2019), 'Optimal design of a fractional-order proportional-integer-differential controller for a pneumatic position servo system', *IEEE Transactions on Industrial Electronics* **66**(8), 6220–6229.

[Ren, Wang, Fan & Kaynak (2019)] Ren, H., Wang, X., Fan, J.-T. & Kaynak, O. (2019), 'Fractional order sliding mode control of a pneumatic position servo system', *Journal of the Franklin Institute* **356**, 6160–6174.

[Romanowski et al. (2006)] Romanowski, A., Grudzien, K., Aykroyd, R.G. and Williams, R.A. (2006), 'Advanced statistical analysis as a novel tool to pneumatic conveying monitoring and control strategy development,' *Particle & Particle Systems Characterization* **23(3-4)**, 289-296.

[Saleem & Abbas (2017)] Saleem, O. & Abbas, F. (2017), Nonlinear self-tuning of fractional-order PID speed controller for PMDC motor, *in* '2017 13th International Conference on Emerging Technologies (ICET)', Islamabad, Pakistan, pp. 1–6.

[Saleem et al. (2020)] Saleem, O., Awan, F., Mahmood-ul Hasan, K. & Ahmad, M. (2020), 'Self-adaptive fractional-order LQ-PID voltage controller for robust disturbance compensation in DC-DC buck converters', *International Journal of Numerical Modelling: Electronic Networks, Devices and Fields* **33**.

[Saleem & ul Hasan (2019)] Saleem, O. & ul Hasan, K. M. (2019), 'Robust stabilisation of rotary inverted pendulum using intelligently optimised nonlinear self-adaptive dual fractional-order pd controllers', *International Journal of Systems Science* **50**(7), 1399–1414.

[Satpati et al. (2014)] Satpati, B., Koley, C., Bhowmik, P. S. & Datta, S. (2014), Nonlinear model predictive control of pneumatic conveying and drying process.

[Shang et al. (2009)] Shang, W., Cong, S., Li, Z. & Jiang, S. (2009), 'Augmented nonlinear pd controller for a redundantly actuated parallel manipulator', *Advanced Robotics* **23**, 1725–1742.

[Shekher et al. (2012)]Shekher, V., Rai, P. & Prakash, O. (2012), 'Tuning and analysis of fractional order pid controller', *International Journal of Electronic and Electrical Engineering* **5**(1), 11–21.

[Sun et al. (2022)] Sun, C., Wang, P., Wang, Q., Chen, Y., & Lin, Z. (2022), 'Flow Control of Pneumatic Conveying System Based on Fuzzy PID', *2022 China Automation Congress (CAC)*, Xiamen, China, 5413-5418,

[Weber and Molerus (1990)] Weber, M., & Molerus, O. (1990), 'Improving the Efficiency of Pneumatic Conveying Systems,' *Powder Handling and Processing* **2(3)**, 249-256.

[Wilms and Dhodapkar (2014)] Wilms, H., & Dhodapkar, S. (2014), 'Pneumatic conveying: optimal system design, operation and control', *Chemical Engineering* **121(10)**, 59.

[Wypych (1995)] Wypych, P.W. (1995), 'Handbook of Pneumatic Conveying Engineering', CRC Press.

[Xu et al. (2018)]Xu, J., Lian, Z., Hu, J. & Luo, M. (2018), 'Prediction of the maximum erosion rate of gas-solid two-phase flow pipelines', *MDPI* **11**(10).

[Yan (1996)] Yan, Y. (1996), 'Mass flow measurement of bulk solids in pneumatic pipelines', *Measurement Science and Technology* **7**(12), 1687–1706.

[Yan (2005)] Yan, Y. (2005), 'Continuous measurement of particulate emissions', *IEEE Instrumentation Measurement Magazine* **8**(4), 35–39.

[Yan et al. (1995)] Yan, Y., Byrne, B., Woodhead, S. & Coulthard, J. (1995), 'Velocity measurement of pneumatically conveyed solids using electrodynamic sensors', *Measurement Science and Technology* **6**(5), 515–537.

[Yan et al. (2021)] Yan, Y., Hu, Y., Wang, L., Qian, X., Zhang, W., Reda, K., Wu, J. & Zheng, G. (2021), 'Electrostatic sensors - their principles and applications', *Measurement* **169**, 108506.

[Yang et al. (2022)] Yang, H., Bewley, G. P. & Ferrari, S. (2022), 'A fast-tracking-particle-inspired flow-aided control approach for air vehicles in turbulent flow', *Biomimetics* **7**(4).

[Yuan and Gao (2019)] Yuan, W. & Gao, G. (2019), 'Disturbance observer–based adaptive integral sliding mode control for the hybrid automobile electro-coating conveying mechanism', *International Journal of Advanced Robotic Systems*, **16**(3), p.1729881419844126.

[Zhang & Pi (2012)] Zhang, B. T. & Pi, Y. (2012), 'Robust fractional order proportion-plus-differential controller based on fuzzy inference for permanent magnet synchronous motor', *IET Control Theory Applications* **6**(6), 829–837.

[Zhang et al. (2012)] Zhang, J., Hu, H., Dong, J. & Yan, Y. (2012), 'Concentration measurement of biomass/coal/air three-phase flow by integrating electrostatic and capacitive sensors', *Flow Measurement and Instrumentation* **24**, 43–49.

[Zhang et al. (2016)] Zhang, S., Yan, Y., Qian, X. & Hu, Y. (2016), 'Mathematical modeling and experimental evaluation of electrostatic sensor arrays for the flow measurement of fine particles in a square-shaped pipe', *IEEE Sensors Journal* **16**(23), 8531–8541.

[Zulkiflli et al. (2019)] Zulkiflli, N. A., Ibrahim, S., Rahiman, M. H. F., Pusppanathan, J., Rahim, R. A., Tee, K. S., Phang, F. A., Nawi, N. D. & Ayob, N. M. N. (2019), Ultrasound tomography hardware system for multiphase flow imaging, *in* '2019 IEEE International Conference on Signal and Image Processing Applications (ICSIPA)', Kuala Lumpur, Malaysia, pp. 264–268.